Elucidating Capacitance and Resistance Terms in Confined Electroactive Molecular Layers

Paulo R. Bueno,*,[†] Francisco Fabregat-Santiago,[‡] and Jason J. Davis*,[§]

[†]Instituto de Química, Universidade Estadual Paulista, CP 355, 14800-900 Araraquara, São Paulo, Brazil

[‡]Grup de Dispositius Fotovotaics i Optoelectrònics, Departament de Física, Universitat Jaume I, Av. Sos Baynat, s/n, 12071 Castelló de la Plana, Spain

[§]Department of Chemistry, University of Oxford, South Parks Road, Oxford OX1 3QZ, England

ABSTRACT: Electrochemical analyses on confined electroactive molecular layers, herein exemplified with electroactive self-assembled monolayers, sample current contributions that are significantly influenced by additional nonfaradaic and uncompensated resistance effects that, though unresolved, can strongly distort redox analysis. Prior work has shown that impedance-derived capacitance spectroscopy approaches can cleanly resolve all contributions generated at such films, including those which are related to the layer dipolar/electrostatic relaxation characteristics. We show herein that, in isolating the faradaic and nonfaradaic contributions present within an improved equivalent circuit description of such interfaces, it is possible to accurately simulate subsequently observed cyclic voltammograms (that is, generated current versus potential patterns map accurately onto frequency domain measurements). Not only does this enable a frequency-resolved quantification of all components present, and in so doing, a full validation of the equivalent circuit model utilized, but also facilitates the generation of background subtracted cyclic voltammograms remarkably free from all but faradaic contributions.
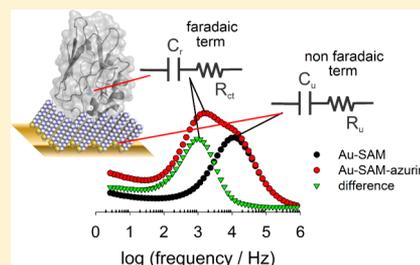
The analysis of interfacial electron transfer characteristics in electroactive self-assembled monolayers (SAMs) is motivated by the removal of the commonly limiting diffusion effects present in conventional electron transfer solution-phase studies[1] and has laid important foundations relevant to the progression of fundamental electron transfer principals and molecular electronics. The dc cyclic voltammetric (linear sweep electrochemistry) analysis of a surface-confined redox couple can, however, be complicated if large background currents (see Figure 1) and/or resistive effects are present. Redox analyses may specifically be distorted by the effects of uncompensated resistance, R_u, causing an iR_u drop additional to that classically related to solution resistance, iR_s. The latter series resistance is a sensitive function of electrochemical cell features, and the intrinsic electrolyte resistance terms are removed from the properties of the SAM itself.[2] Together, these nonfaradaic contributions can be limiting in terms of producing visibly nondistorted signals, and they are responsible for significant miscalculation in derived kinetic analyses.[2] These effects may be particularly marked within bioelectronic analyses where faradaic current densities can be such (weak) that the signal is effectively lost within this "noise".[2,3] It has additionally been shown, for example, by means of the classical and phenomenological Butler–Volmer analysis, that the effects of non-negligible, uncompensated resistance (between 1.5 and 2 kΩ[4]) in cyclic voltammetry (CV) analysis (see Figure 1a) can distort plots of peak current versus voltage sweep rate, such that the i_p versus v linear trend, commonly touted as being diagnostic of an adsorbed redox couple, is not observed.[4a]

Depending on the magnitude of these effects, current versus voltage trends may sit midway between expectations of diffusive or surface-confined redox couples,[4] that is, to be nonlinear. These distortions, which can lead to erroneous kinetic or thermodynamic interpretations of SAM-based electron transfer, are often subtle and easily overlooked.[2,4a] Capacitive background terms present an additional problem.[5]

There is, then, a need to both better understand the contributions to measured current in such experiments and to establish a more robust means of segregating faradaic contributions from those which we may regard as "parasitic" or distorting (i.e., combined resistive and capacitive terms) (see Figure 2). The role played by the supportive dielectric SAM layer existing between the electrode and redox centers should be considered in any proposed methodology.[6]

With this need in mind, alternating current ac voltammetry has, for example, been used at high ac frequency[2,3] to resolve electron-transfer dynamics specifically within surface-confined films.[2,3,7] An interpretation of the current response within these nonlinear methods remains challenging, however, and partially related to the large capacitive double layer contributions in experiments when the voltage waveform changes rapidly.[5] Though the latter can be elegantly suppressed through Fourier-transform processing, the results are instrumentally controlled and empirically modeled and, accordingly, lend themselves less
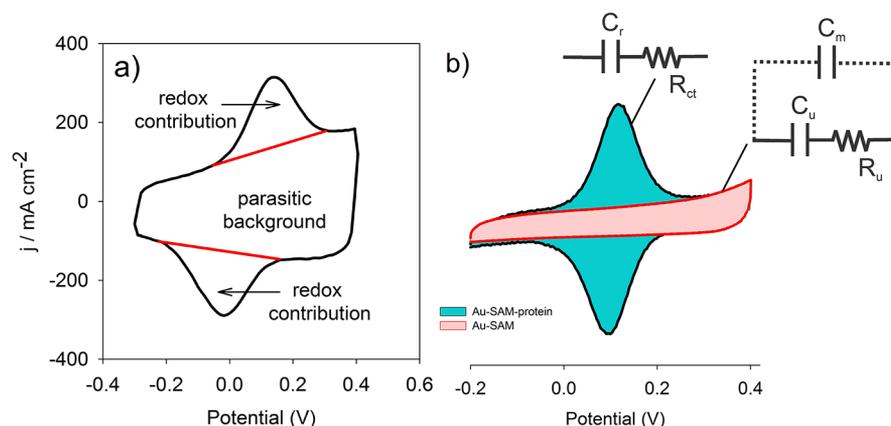
Figure 1. (a) A typical experimental CV analysis of a surface-confined reversible redox system comprising a protein film (here the blue copper protein azurin) on a supportive dodecanethiol SAM. The large background current contribution, caused by a distorting "parasitic" response, is highlighted. The voltage scan rate and reference are 100 mV s^{-1} and calomel (SCE), respectively. (b) Another representative experimental cyclic voltammogram (different shape from the previous) of a surface-confined reversible redox system comprising a protein film in which the dominant equivalent circuit parameters responsible for current are depicted in terms of faradaic (R_{ct} and C_r) and nonfaradaic (C_m, R_u, and C_u) components. The capacitance element of the supporting monolayer, C_m (see text and ref 6 for more detail), does not generate a significant contribution at any potential, as will be discussed and demonstrated herein.
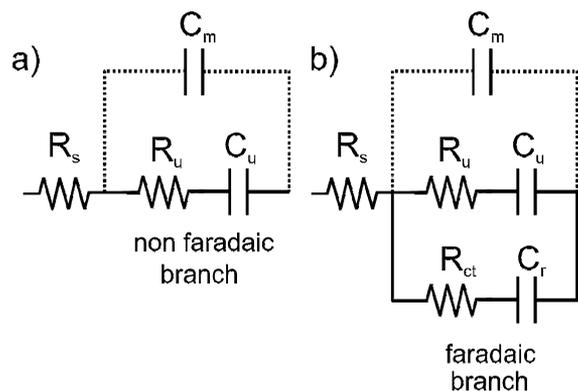

Figure 2. (a) The proposed equivalent circuit model of a self-assembled monolayer that considers dipolar/electrostatic effects, where R_u and C_u are uncompensated resistance and capacitance, respectively. (b) The same as (a) but with SAM-associated redox centers {i.e., with faradaic contribution represented by an additional resistive/capacitive branch in which C_{ct} is the charge-transfer resistance, C_r is the redox capacitance, R_s is the solution or electrolyte resistance, and C_m is the pure electronic capacitance [i.e., the monolayer capacitance without ionic contribution (the share-out lines indicate that the contribution of this term is low)]}.

readily to either standard voltammetric methods or a clearly interpreted physical depiction of the electrode interface.

We have recently introduced capacitance spectroscopy (CS) as a means of mapping the faradaic and kinetic features of electroactive monolayers (something we have termed electroactive monolayer capacitance spectroscopy[6] or EMCS[8]), as well as the dipolar/electrostatic features of nonelectroactive SAMs (capacitance spectroscopy or SAMCS).[6] The latter theoretical framework, exemplified across a range of alkanethiol films,[6] is fully aligned with, but more detailed than, the classic Helmholtz plate capacitor model of such interfaces and resolves trends in capacitance and distorting resistance effects (a more elaborate model) as a function of film thickness.[6]

The goal of the present work is to extend this initial work in demonstrating that spectrally resolved voltammetric contributions can not only be visualized by capacitance spectroscopy

but also subsequently used in the independent construction of "normal cyclic voltammograms", background cyclic voltammograms (our electroactive monolayer reference system was azurin-on-thiol films), and background-subtracted cyclic voltammograms from which the effects of uncompensated resistance and additional capacitive effects have been removed. Finally, the methodology is applied to the precise simulation of the effects of charge-transfer resistance and redox capacitance.

■ EXPERIMENTAL PROCEDURE

Polycrystalline gold disk electrodes (GDE) (Cypress Gold, diameter 1 mm) were cleaned following a published procedure[9] and immersed in a 1 mM octanethiol $(CH_2)_8$ and dodecanethiol $(CH_2)_{12}$ (Sigma-Aldrich) solution in HPLC-pure ethanol (overnight, room temperature). Electrodes were then rinsed with ethanol and water and dried under nitrogen. Subsequent protein (azurin) physisorption on the hydrophobic SAM surface was facilitated by incubating 5 μL aliquot of 0.5 mM protein in 20 mM MES [2-(N-morpholino)ethanesulfonic acid] buffer at pH 7.0 for 30 min. The so-modified electrode was then rinsed with buffer and immersed in the electrochemical cell. Cyclic voltammetry (CV) and electrochemical impedance spectroscopy (EIS) measurements were carried out using a PC-controlled Autolab potentiostat PGSTAT20 (Ecochemie NL) equipped with an ADC750 and a FRA (Frequency Response Analyzer) module. Alternating current frequencies ranged from 1 to 10 mHz, with an amplitude of 10 mV. The potential sweep for EIS analysis was from −100 to 300 mV with a 50 mV step. All the obtained impedance data were checked regarding compliance with the constraints of linear systems theory by Kramers−Kronig using the appropriate routine of the FRA AUTOLAB software. All electrochemical measurements were within a 5 mL volume one compartment cell containing the GDE, a saturated calomel reference (SCE), and a platinum gauze as the counter electrode. As a supporting electrolyte, 200 mM $NaClO_4$ and 5 mM MES, in ultrapure water (18.2 MΩ on a Milli-Q system from Millipore Corp.) buffered at pH 5.0 with NaOH, was used. All the solutions were deoxygenated by bubbling argon and purging the surface of the electrolyte for the duration of the experiment. The complex Z*
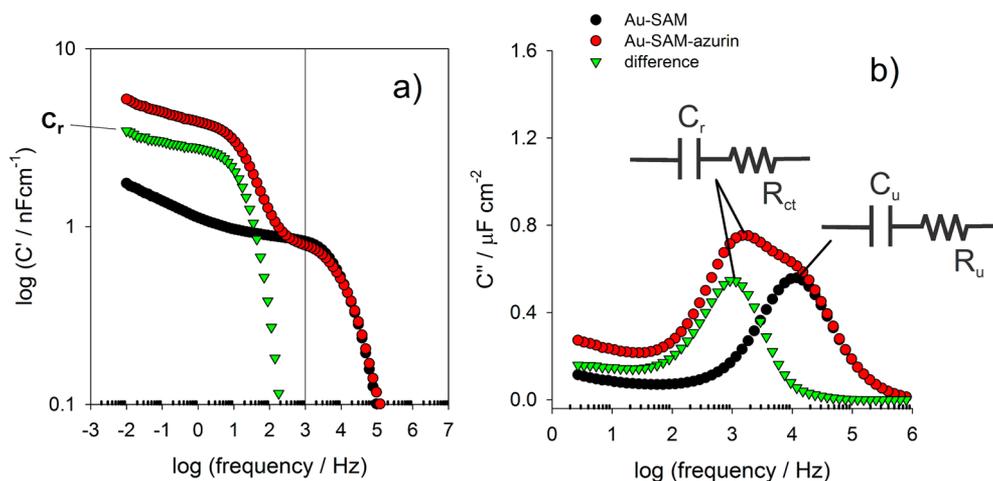
Figure 3. A (a) real and an (b) imaginary component of a Bode capacitance plot illustrating the frequency-resolved components (red) and their subsequent subtraction (into green and black). The faradaic and main nonfaradaic term contributions to the response are illustrated in (b).
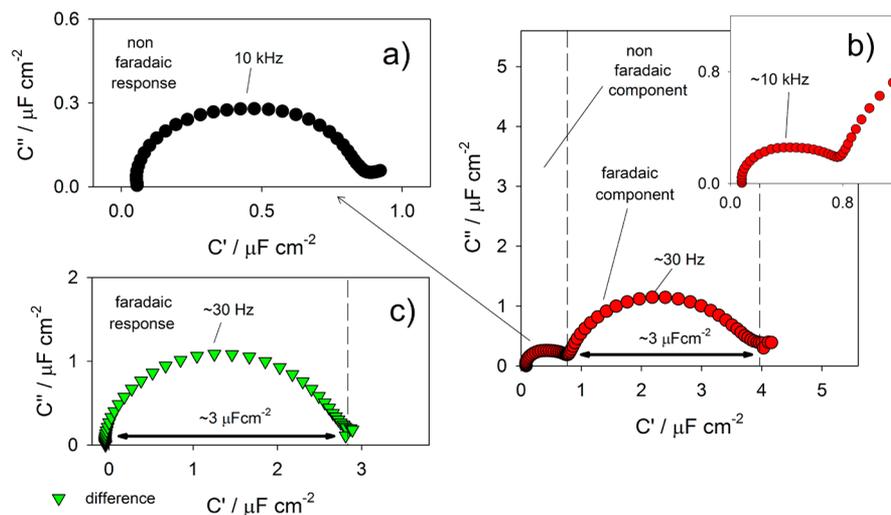

Figure 4. Nyquist capacitive plots of CS analysis with the electrode potential poised (a) outside of the redox window where the response is dominated nonfaradaic processes (here of an azurin-on-dodecanethiol film) and (b) at the electrochemical reversible potential (i.e., with the electrode poised inside redox window). The resultant CS spectrum [a subtraction of (a) from (b)] is shown in (c), where the nonfaradaic contribution is corrected and only one semicircle remains. The inset in (b) corresponds to a magnification of the high-frequency spectral region. In (c), it is shown with the same data of (b) after subtraction of the "parasitic" nonfaradaic response. The successful subtraction of uncompensated resistance and nonfaradaic contribution in (c) can be demonstrated by the total elimination of relaxation observed in (b) (magnified in the inset), where this signal is totally absent.

(impedance) function was converted into C^* (capacitance) through $Z^* = 1/j\omega C^*$, in which ω is the angular frequency. The impedance and capacitance data were fit to the equivalent circuit from Figure 2 using ZView software (Scribner Associates Inc.).[10] Simulated CV curves were constructed from parameters acquired from the fitting of frequency response data to the equivalent circuit models of Figure 2 (that consider the additional nonfaradaic and faradaic terms). The circuit of Figure 2a, as expected, dominates the current response at potentials outside redox windows with the model of Figure 2b prevailing inside at potentials inside redox windows (i.e., here from 50 to 200 mV vs SCE) (see Figure 1b). The magnitude of each parameter was obtained for steady-state potentials spanning from −100 to 300 mV versus SCE and, from these, current as a function of potential mapped. The generated CVs (time domain data obtained from frequency domain data) were then compared to those experimentally obtained for the same electroactive monolayer system. Significantly, there was no

steering or guiding of the simulations through this comparison. The evolution of current with scan rate was then simulated using the previously optimized resistive and capacitative parameters.

■ RESULT AND DISCUSSIONS

Identifying Capacitive and Resistive Terms. As stated in a previous work,[8] CS resolves the capacitance and resistance features (in either Bode, Figure 3, or Nyquist diagrams, Figure 4) that represent a dipolar/electrostatic fingerprint of molecular films and enables monolayer capacitance and resistance to be directly determined.[8] The resistive term, R_u, representing an ionic resistive feature of the SAM (the electronic resistance is unresolved on timescales accessible with a potentiostatic measurement), couples with an associated capacitive term, C_u, arising from ionic ingress into the film, to contribute to a resolvable time constant for ionic relaxation (illustrated herein

in Figure 2a and Figure 3a, dark curve). Since C_u and this timescale are spectrally resolved,[8] R_u is then calculated. This intrinsic resistance is a source of potential drop[6] and can make a significant contribution to the uncompensated resistance.[6] In previous work, we have noted the dependence of this on monolayer thickness.[6] The equivalent circuit of Figure 2a thus depicts a resolved modification of the simple, classic, interfacial Helmholtz model in the presence of a monolayer film spanning between the solid (electronic) and the electrolyte (ionic).[6] It is important to note that this model is more detailed and contains more terms than that proposed by Creager et al.[11] in providing a clear physical origin of the resolved capacitance term (representing dipolar ionic monolayer features and a term previously referred to as adsorption capacitance);[11] we demonstrate herein that the latter is, in fact, a redox process with a magnitude directly related to the accessibility of redox-site density of states. It is important to mention that, while C_u is the bulk capacitance of the monolayer (the expected layer capacitance with ionic ingress), C_m is the expected capacitance of the layer without electrolyte or protons (or cations), quantitatively lower than C_u.

The main results from the fitting impedance/capacitance data to the models of Figure 2 across a range of applied potentials will be further introduced and discussed herein (see Figure 6 for an earlier analysis). Note that there, R_s and R_u are nearly constant with 0.2 Ω cm^2 and 15 Ω cm^2, respectively.

When a redox component is incorporated into or added to such films, additional resistance (R_{ct}) and capacitance (C_r) terms, related to faradaic activity, are introduced and separately resolved (a process constituting EMCS), where the terms previously detected by SAMCS constitute distorting elements of faradaic activity that can be subtracted.

A fundamental starting point in spectrally resolving the sum total of redox, electrostatic, and ionic dipolar contributions present at a molecular film-modified electrode is the analysis of complex capacitance, $C^*(\omega)$, as represented within either a Bode (see Figure 3) or a Nyquist plot (Figure 4). Experimentally, this is a simple steady-state approach from which a precise resolution of electron transfer kinetics (directly from the peak frequency of the redox process observed in Figure 3b) is obtained from only a single capacitance/impedance sampling inside the film redox window and one outside. In the latter, the capacitive and resistive dielectric features of the monolayer, in addition to the IR_s term, are spectrally resolved in one step (see Figures 2b and 3), constituting a background response that can subsequently be subtracted from the redox data acquired within the redox window potential (see Figures 2b and 3).

In these analyses (Figure 3b), the characteristic timescale of faradaic and nonfaradaic processes are directly resolved (i.e., the frequency of the peak of imaginary component of the complex capacitance (C'') corresponds to $\tau_r^{-1} = R_{ct}C_r$ and $\tau_r^{-1} = R_uC_u$ for faradaic and nonfaradaic processes, respectively. Once these characteristic timescales are obtained by means of Bode plots of the imaginary component (see Figure 3b), the capacitance values of C_u and C_r are readily obtained from either Bode (real component analysis, Figure 3a) or Nyquist (Figure 4) graphical analyses. The associated resistive terms (R_{ct} and R_u) can subsequently be obtained from the numerical relationship between resolved time constant and RC.

If the faradaic and nonfaradaic timescales are comparable (as may be the case for a very fast redox couple), the individual capacitive peaks will be convoluted and analysis potentially difficult. In previous work,[8] we have, however, demonstrated a simple and effective means of resolving these individual components. To exemplify this here, we look at capacitive data associated with an azurin-on-dodecanethiol film (Figure 4). Here, the timescales associated with nonfaradaic and faradaic processes are resolved in the Nyquist diagram of Figure 4 (panels a and c) to be approximately 10 kHz (0.1 ms) and 30 Hz (~33 ms), respectively. For an equivalent film on a shorter alkyl dielectric SAM (octanethiol), the nonfaradaic relaxation is around 15 kHz (~0.07 ms) while the redox process is around 1 kHz (1 ms), largely reflecting a lower R_{ct}.[8] The corresponding redox-only capacitive fingerprint is acquired at the reversible redox potential and subsequently cleaned by subtraction (Figure 4c).

Thus far, we have presented an improved equivalent circuit model that both considers all terms contributing to the measured current in electrode-confined SAMs and is underpinned by spectrally resolved capacitance analysis. It is then possible to quantify all equivalent circuit components, that is capacitive terms derived directly from capacitive Nyquist and resistance obtained subsequently from Bode plot timescales. In the following sections, a utilization of this frequency-domain resolving power in simulating (and thus interpreting) linear-sweep voltammetric responses will be demonstrated.

Simulating Acquired Cyclic Voltammetry. As impedance/capacitance spectroscopic experiments constitute steady-state analyses, current variations over time (or indeed voltage sweep rate) can be simulated by analyzing how the constitutive capacitive and resistive terms (faradaic and nonfaradaic) of the system respond as a function of time. This information is directly acquired as detailed in the Experimental Procedure and mapped onto the model of Figure 2.

The equivalent circuit shown in Figure 2a was used to fit the CS data acquired outside the redox window, while that in Figure 2b was used for CS data obtained at potentials inside. In other words, once the resistive and capacitive contributions (resistive and capacitive terms) were resolved in the frequency domain, the time-dependent responses are modeled (see Experimental Procedure), prior to comparison with experimentally acquired CV data. Figure 5 summarizes the results of this at two voltage scan rates, showing both CVs simulated from impedance/capacitance analysis (red lines) and those acquired independently by experiment (black lines). It is
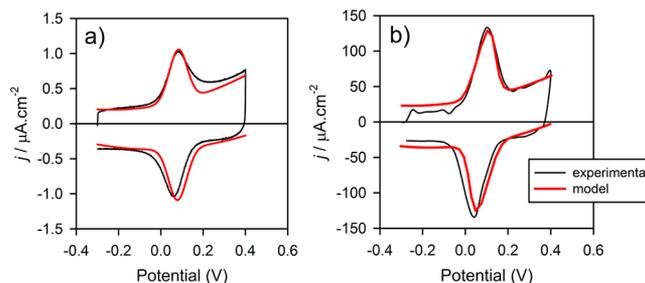

Figure 5. Comparison of experimental and simulated cyclic voltammetric patterns. The latter were obtained from the CS/EIS parameters after fitting to the equivalent circuit shown in Figure 2 (that considers the dipolar/electrostatic features of the monolayer for potentials outside the redox windows and additional redox terms when the steady-state potential is inside the redox windows) of the azurin-on-octanethiol films. (a) Cyclic voltammetry obtained/generated at 4 mV/s and (b) at 1200 mV/s scan rates.
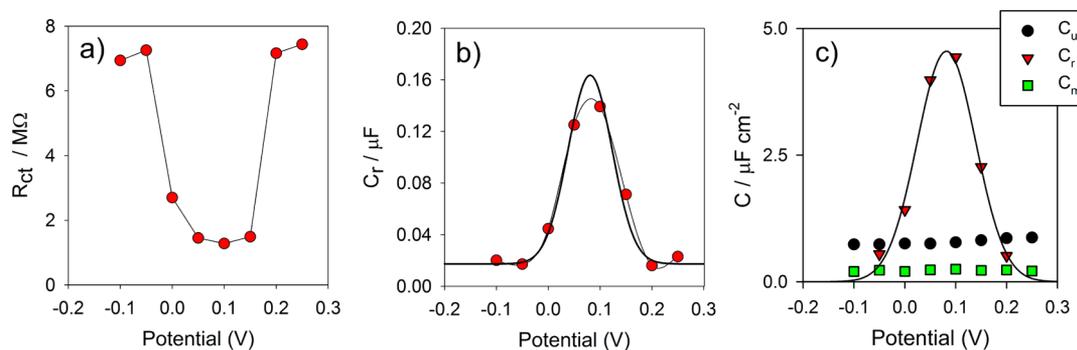
Figure 6. (a) Charge transfer resistance as a function of potential, as obtained from fitting the impedance/capacitance data to the equivalent circuits of Figure 2b, showing that the minimum value is around the reversible potential for any fixed SAM thickness. (b) Redox capacitance (Gaussian-fitted in black) as a function of the potential obtained (in red) from impedance/capacitance data fitted to equivalent circuit of Figure 2b at different steady state potentials. This capacitance controls the redox current according to eq 1 and, as discussed in the main text, directly reports on the interaction of the electrode Fermi−Dirac distribution with the redox site DOS. Through the potential dependence of this interaction (charging), the C_r function directly controls voltammetric peak shape. (c) The comparison of the magnitude of all capacitive terms as a function of potential with respect to C_r, showing that C_r dominates over the others on redox windows potential.

evident that the simulations, based purely on generating time-domain data for all components of the equivalent circuits outlined in Figure 2, lie in excellent agreement with the experimental observations of current−voltage trends.

In the next section, we return to the components of the equivalent circuit, paying special attention to the meaning of C_r and both its direct reporting of faradaic activity and its contribution to peak current in CVs.

Since C_m is small,[6] it can reliably be disregarded and the total capacitive current density, j, is then the sum of two contributions, the faradaic (j_f) and nonfaradaic (j_u) according to

$$j_f = \frac{dq_r}{dt} = C_r \frac{dv}{dt} = C_r s \qquad (1)$$

and

$$j_u = \frac{dq_e}{dt} = C_u \frac{dv}{dt} = C_u s \qquad (2)$$

where all capacitances are per unit of area. V is the potential with respect to the reference electrode (note that the true electrode potential is $V - i(R_u + R_s)$ for nonfaradaic contribution, and $V - i(R_{ct} + R_s)$ for faradaic, assuming that the two resistive nonfaradaic terms are responsible for iR drop as stated in the introduction[12]) and $s = dV/dt$ is the potential scan rate. $q_r = ne$ is the redox charge associated with the redox centers and e is the elementary charge, where n is the number of occupied redox centers. It is important to note that C_r is not a common electrostatic capacitance whose potential depends exclusively on the dimension of the capacitor. It is, rather, a redox capacitance, whose occupation/magnitude depends on redox center occupancy. q_e is the electrostatic charge of the monolayer (with its ionic contribution included[6]).

As demonstrated in a previous work, the magnitude of R_u is expected to depend linearly on the thickness of the SAM dielectric.[6] Conversely, R_{ct} is expected to increase exponentially with the same, since it is specifically reflective of redox site-electrode electronic coupling [according to $1/R_{ct} \propto \exp(-\beta L)$, where β is a constant (the "distance decay parameter"), and L is the monolayer thickness]. For any given L, R_{ct} is a minimum at the reversible electrode potential as shown in Figure 6b.

Once we have acknowledged the physical basis of these circuit components, we can examine how they make direct contributions to experimental observations in CV.

Subtracted cyclic Voltammograms: Charge Transfer Resistance and Redox Capacitance Effects. In the previous section, we acknowledged the physical origin of the resistive terms that contribute to and potentially distort voltammetric analyses and, additionally, noted that it is the capacitive term, C_r, that reports directly on the efficacy of the redox charge transfer. The population of this term (the CV peak) is dependent on Fermi−Dirac statistics in a way that nonfaradaic contributions, such as that involved with ionic relaxation, are not. Specifically, the faradaic current, j_f, depends on the potential according to $f = n/\Gamma = F(E_r, \mu_e)$ and the redox group surface density/coverage, Γ, as stated in previous work[8] where

$$f = F(E_r, \mu_e) = \frac{1}{1 + \exp[(E_r - \mu_e)/k_B T]} \qquad (3)$$

E_r is the formal potential of redox states, and μ_e is the electron chemical potential (or the Fermi level, E_F) that is related to the electrode potential V by

$$dV = -\left(\frac{1}{e}\right) d\mu_e \qquad (4)$$

From the derivative of eq 3, it is possible to define C_r for a single redox energy state E_r, as[8,13]

$$C_r = e^2 \Gamma \frac{df}{d\mu_e} = \frac{e^2 \Gamma}{k_B T} f(1 - f) \qquad (5)$$

Note the correspondence (by combining eq 1 and 5) between CV-resolved peak current (faradaic activity) and the redox occupation function, $f = n/\Gamma$, that then, according to eq 1, presents a maximum value of C_r when $f = 1/2$ and $f(1 - f) = 1/4$.

If one considers, more realistically, a distribution of states, $D(E)$ around E_r, instead of a single redox energy state, the redox capacitance is obtained integrating over the contributions of all available energy states, thus[8,13]

$$C_r(\mu_e) = e^2 \int_{\infty}^{-\infty} D(E) \frac{df}{d\mu_e} dE$$

$$= \frac{e^2 \Gamma}{k_B T} \int_{\infty}^{-\infty} D(E) f(1-f) dE \tag{6}$$

In assuming the zero-temperature approximation for Fermi−Dirac statistics then

$$C_r(\mu_e) = e^2 D(E) \tag{7}$$

(i.e., the redox capacitance is proportional to the density of states (DOS), $D(E)$. Finally, $D(E)$ can be written as

$$D(E) = \frac{1}{\sigma\sqrt{2\pi}} \exp\left[-\frac{E_r - E}{2\sigma^2}\right] \tag{8}$$

Since a distribution of E_r will be represented by a Gaussian function reporting on the spread, we see in combining eqs 7 and 8, the same Gaussian function displayed in the trend of C_r with potential (Figure 6b). This enables a resolution of E_r (~82 ± 4 meV versus SCE),[8] σ (57 ± 4 meV) (indicative of a Nernstian distribution of redox states),[8] and finally, as demonstrated in previous work[8] the surface density, Γ (1.6 ± 0.2 pmol cm^{-2}).[8]

Then equations 3 and 7, in contrast to the classic Butler−Volmer phenomenological model, take into account the metallic electrode structure and the coupling of this to electrode-confined redox states. In acknowledging that the C_r component reports purely on the process of faradaic activity, without any associated additional nonfaradaic contributions, we can, in mapping this circuit component across a range of potentials, simulate/generate a "pure" redox CV pattern (see Figure 7, for instance). Note that these are different to the
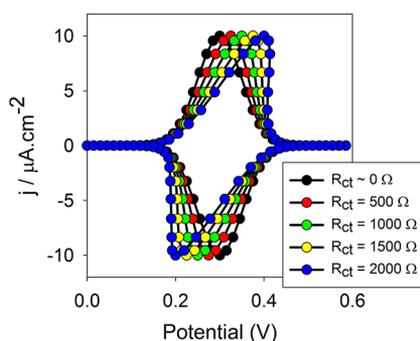

Figure 7. An increase in the thickness of a redox supporting monolayer leads to a linear increase in R_u (which decreases background current) and a linear decrease of C_u.[6] Background-subtracted cyclic voltammograms, generated directly from C_r, are free of the influence of these values but do nicely resolve the impact of increasing R_{ct} (equivalent to a progressively decreased redox site−electrode coupling), where a progressive distortion and peak separation is evident. R_{ct} values are shown (not normalized) for a direct comparison with ref 4a.

simulated CVs of Figure 5, for example, in that only the purely Faradaic contributions are considered. Once we have done this, it is possible to directly examine the effects of redox site−electrode electronic coupling (reported directly through R_{ct}) on wave shape. As stated previously, this resistance term, which of course varies exponentially with electrode surface−redox site separation, has the effect of dropping a component of the applied potential between the electrode surface and the redox

site. The effects of this can be directly simulated within "purely faradaic" CVs (Figure 7).

To summarize, in considering the capacitive and resistive constituents that operate within a surface confined redox active film under an electrolyte, it is possible to isolate purely faradaic responses, accurately simulate experimental observations, and directly examine the effects of electronic coupling on the subsequently observed wave shape.

Though largely empirical attempts have been made in previous work[11] to fit experimentally observed voltammograms to fixed capacitive and resistive contributions, these approaches[3−5,11] have not previously considered either the SAM dielectric terms fully or the potential modification of these individual terms, as components are incorporated into a film prior to analysis; the laying down of a protein on a supporting alkyl thiol SAM, for example, may modify the capacitance associated with the latter "background" CVs obtained, simply by scanning the current−potential characteristics in the absence of the redox element. These are, thus, not viable means of "cleaning" subsequently observed CVs of "parasitic" (i.e., nonfaradaic) current contributions. The model discussed herein, in validating a previously introduced methodology,[8] empowers a physically embodied analysis of redox film voltammetry and the contributions within this, with a clarity that we believe unprecedented.

■ FINAL REMARKS AND CONCLUSIONS

The current generating characteristics of electrode-confined films can be mapped using equivalent circuit terms resolved by capacitance spectroscopy. These constituent terms report on the film dielectric, kinetic, and dipolar features and, in so doing, systematically resolve the additional nonfaradaic contributions inherently present and distorting of, in particular, kinetic analyses (exemplified here with the electroactive copper protein, but the approach is equally applicable to any molecularly confined redox-active interface). We have, within this and previous work, given all terms a physical manifestation and noted, in particular, that C_u represents ionic charge and its field-induced fluctuation within the confined film. These contributions have, to the best of our knowledge, never been clearly resolved by ac or dc voltametric-based techniques. The CVs simulated herein from spectrally resolved circuit components overlay experimental observations with strikingly good agreement (validating the former). Within these simulations, we have explored the effect of progressively increased R_{ct} (decreased electronic coupling) on the shape of subsequently observed voltammograms and noted the origins of voltammetric wave shape (current trends with potential), through C_r, to the Gaussian distribution of redox-state energies. The redox capacitance term, C_r, has a physical meaning that has not been previously acknowledged and thus controls the CV shape acquired from any confined redox molecular film according to eq 1. It can also be utilized in calculating coverage dependent addressable redox site density of states.

Finally, as noted in previous work with comparable objectives,[2−3,5] these contributing terms are present within any confined redox active film. The methodology discussed herein thus provides a broadly applicable theoretical framework, experimentally validated and not tethered to empirical explanations typified by alternative ac or dc voltammetric approaches.

■ AUTHOR INFORMATION

Corresponding Author

*P.R.B.: e-mail, prbueno@iq.unesp.br; tel, +55 16 3301 9642; fax, +55 16 3322 2308. J.J.D.: e-mail, jason.davis@chem.ox.ac.uk; tel, +44 1865 275914.

Notes

The authors declare no competing financial interest.

■ REFERENCES

(1) (a) Eckermann, A. L.; Feld, D. J.; Shaw, J. A.; Meade, T. J. *Coord. Chem. Rev.* **2010**, *254*, 1769−1802. (b) Finklea, H. O. Organized Monolayers on Electrodes. In *Electroanalytical Chemistry*; Bard, A. J.; Rubinstein, I., Eds. Marcel Dekker, Inc.: New York, 1996; Vol. *19*.

(2) Fleming, B. D.; Zhang, J.; Elton, D.; Bond, A. M. *Anal. Chem.* **2007**, *79*, 6515−6526.

(3) Armstrong, F. A.; Butt, J. N.; Sucheta, A. Voltammetric Studies of Redox-Active Centers in Metalloproteins Adsorbed on Electrodes. In *Methods in Enzymology*; Riordan, J. F.; Vallee, B. L., Eds.; Academic Press: San Diego, 1993; Vol. *227*, pp 479−500.

(4) (a) Feldberg, S. W. *Anal. Chem.* **2011**, *83* (15), 5851−5856. (b) Stiles, R. L.; Balasubramanian, R.; Feldberg, S. W.; Murray, R. W. *J. Am. Chem. Soc.* **2008**, *130* (6), 1856−1865.

(5) (a) Bond, A. M.; Duffy, N. W.; Elton, D. M.; Fleming, B. D. *Anal. Chem.* **2009**, *81* (21), 8801−8808. (b) Lee, C.-Y.; Fleming, B. D.; Zhang, J.; Guo, S.-X.; Elton, D. M.; Bond, A. M. *Anal. Chim. Acta* **2009**, *652* (1−2), 205−214.

(6) Góes, M. S.; Rahman, H.; Ryall, J.; Davis, J. J.; Bueno, P. R. *Langmuir* **2012**, *28* (25), 9689−9699.

(7) Stevenson, G. P.; Lee, C.-Y.; Kennedy, G. F.; Parkin, A.; Baker, R. E.; Gillow, K.; Armstrong, F. A.; Gavaghan, D. J.; Bond, A. M. *Langmuir* **2012**, *28* (25), 9864−9877.

(8) Bueno, P. R.; Mizzon, G.; Davis, J. J. *J. Phys. Chem. B* **2012**, *116*, 8822−8829.

(9) Tkac, J.; Davis, J. J. *J. Electroanal. Chem.* **2008**, *621* (1), 117−120.

(10) ZPlot and ZView for Windows Software Downloads; Scribner Associates Inc.: Southern Pines, NC (http://www.scribner.com/zplot-and-zview-for-windows-software-downloads.html).

(11) Creager, S. E.; Wooster, T. T. *Anal. Chem.* **1998**, *70* (20), 4257−4263.

(12) Additionally, herein note that the R_u is equivalent to R_t while C_u is to C_t according to nomenclature of reference 8. The different nomenclature used here is to emphasize that these are, by default, uncompensated terms.

(13) (a) Fabregat-Santiago, F.; Mora-Sero, I.; Garcia-Belmonte, G.; Bisquert, J. *J. Phys. Chem. B* **2003**, *107* (3), 758−768. (b) Bisquert, J.; Fabregat-Santiago, F.; Mora-Sero, I.; Garcia-Belmonte, G.; Barea, E. M.; Palomares, E. *Inorg. Chim. Acta* **2008**, *361* (3), 684−698.

417

dx.doi.org/10.1021/ac303018d | *Anal. Chem.* 2013, 85, 411−417